Journal of Materials Chemistry B

Accepted Manuscript

ROYAL SOCIETY OF CHEMISTRY

www.rsc.org/materialsB

A new bifunctional electrochemical sensor for hydrogen peroxide and nitrite based on a bimetallic metalloporphyrinic framework

Li-Mei Shi, Jing-Xiong Pan, Bo Zhou*, Xiaoqing Jiang*

Jiangsu Key Laboratory of New Power Batteries, National-Local Joint Engineering Research Center for Biomedical Functional Materials, Jiangsu Collaborative Innovation Center of Biomedical Functional Materials, Jiangsu Key Laboratory of Biomedical Materials, College of Chemistry and Materials Science, Nanjing Normal University, Nanjing 210023, 1 Wenyuan Road, P. R. China

*Corresponding authors: Bo Zhou, Xiaoqing Jiang

E-mail: zhoubo@njnu.edu.cn, jiangxiaoqing@njnu.edu.cn

Phone number: +86 25 85891707

Fax: +86 25 85891767

Postal address: College of Chemistry and Materials Science, Nanjing Normal University, Nanjing 210023, 1 Wenyuan Road, P. R. China.

Abstract:

Metalloporphyrinic frameworks have been studied in many fields. However, their electrochemical properties were seldom reported. This work reports the synthesis and the electrochemical application of a new bimetallic metalloporphyrinic framework, $[Cu_2\text{-}Co[5,10,15,20\text{-}(4\text{-carboxyphenyl})porphyrin](H_2O)_2]\cdot 0.5DMF\cdot 5H_2O$ (Cu-CoTCPP) in which [5,10,15,20-(4-carboxyphenyl)porphyrin]Co(II) (CoTCPP) struts are bound by Cu(II)-carboxylate clusters ($Cu_2(COO)_4$). Cu-CoTCPP was synthesized by solvothermal method and characterized by various techniques, including XRD, IR, UV-vis, elemental analysis, TG, and TEM. Cu-CoTCPP showed novel bifunctional electrocatalytic ability toward the reduction/oxidation of H_2O_2 and the oxidation of $NaNO_2$, which might be due to Cu and Co central ions, respectively. With the assistance of multi-walled carbon nanotubes (MWCNTs), Cu-CoTCPP showed further improved sensing performance toward H_2O_2. The linear detection ranges of Cu-CoTCPP/MWCNTs/GCE for H_2O_2 and $NaNO_2$ are $5.0\times10^{-7} \sim 1.8\times10^{-4}$ M and $2.5\times10^{-6} \sim 1.1\times10^{-3}$ M, respectively, with detection limits of 2.4×10^{-7} M and 1.7×10^{-7} M, and sensitivity of 168 and 439 mA mol^{-1} L cm^{-2}. The bifunctional electrocatalytic ability and the excellent performance imply that the metalloporphyrinic frameworks are promising candidates for fabricating electrochemical sensors.

Keywords: bimetallic metalloporphyrinic frameworks, electrochemical sensing, hydrogen peroxide determination, nitrite determination

1. Introduction

In recent two decades, metal-organic frameworks (MOFs) have received tremendous attention owing to their powerful attributes on structural and chemical versatility and tailorability [1]. Such materials have been examined for storage, separations, sensors, size and shape-selective catalysis, molecular recognition, and nanoscale reactors [2-6]. Metalloporphyrin molecules are excellent candidates to act as components of molecular building blocks for the construction of MOFs, because of various functional group substituents in the periphery of the molecule and the huge variety of available derivatives incorporating different centre-coordinated metals, thereby allowing fine control of the linkage motif [7]. Crystals of MOFs with porphyrin molecules as building blocks [8, 9] have been successfully synthesized and their highly selective adsorption [10] and catalytic properties [11] have been reported. However, the electrochemical catalytic property of metalloporphyrinic frameworks is still rarely investigated.

Metalloporphyrins are very stable π-conjugated macrocyclic molecules forming a diverse class of multifunctional materials, which exhibit interesting and useful catalytic, optical, electronic and biological properties [12]. Therefore, metalloporphyrins have potential application in electrochemical sensing. Attracted by the high biomimetic catalytic efficiency of metalloporphyrins [13, 14] and various valence states and electrochemically active of copper/cobalt, porphyrin, copper and cobalt were selected to synthesize a bimetallic metalloporphyrinic framework. A new bimetallic MOF, [Cu_2-Co [5,10,15,20-(4-carboxyphenyl)porphyrin]

$(H_2O)_2]\cdot 0.5DMF\cdot 5H_2O$ (Cu-CoTCPP) was successfully synthesized hydrothermally in this work. This Cu-CoTCPP was successfully used to fabricate electrochemical sensors. Multi-walled carbon nanotubes (MWCNTs) were used to further improve the performance of the sensors.

Hydrogen peroxide (H_2O_2) is an important signal molecule in many biological processes. Therefore the accurate determination of H_2O_2 is a hot topic in biosensing. Nitrite (NO_2^-) has been widely used as a corrosion inhibitor and an additive in foods and physiological systems. Hence, effective determination of NO_2^- is of great importance for public health. Comparing with those traditional methods, which are based on spectrophotometry [15, 16], fluorescence [3, 17], or chemiluminescence [18, 19], electrochemical technique is simple, fast, low-cost, convenient and sensitive, and has been extensively employed in H_2O_2 and NO_2^- determination. For example, Hua et al. reported a sensor based on a horseradish peroxidase/polyaniline/MWCNT for detecting H_2O_2 [20] and Hu et al. fabricated a sensor based on reduced graphene oxide and MWCNT hybrid to detect NO_2^- [21]. Only a very few coordination polymers have been used as electrocatalysts [22, 23]. The MOFs cooperating with MWCNTs have been rarely reported in areas of modified electrodes [24]. In this work, a bimetallic MOF, Cu-CoTCPP/MWCNTs, was applied to construct a novel sensor for H_2O_2 or NO_2^- with good performance. To our knowledge, Cu-CoTCPP provides the first example of bimetallic MOF toward the electrocatlysis of H_2O_2 or $NaNO_2$.

2. Experimental

2.1 Reagents

All reagents were analytical pure and used as purchased without further purification. The 5,10,15,20-(4-carboxyphenyl)porphyrin (H_2TCPP) and [5,10,15,20-(4-carboxyphenyl)porphyrin]Co(II) (CoTCPP) ligand were synthesized according to previous reports [25, 26]. Typically, pyrrole (20 mmol) and ethoxycarbonylbenzaldehyde (20 mmol) were added quickly in boiling propionic acid (160 mL). The mixture was refluxed for 2 h. The obtained crude product (H_2TCPP) was washed with alcohol and purified by flash chromatograph. Then H_2TCPP (0.1 mmol) and $CoCl_2 \cdot 6H_2O$ (0.5 mmol) were added in 50 mL DMF and refluxed for 12 h. The product (CoTCPP-OMe) was washed with water.

2.2 Equipment and apparatus

Powder X-ray diffraction (XRD) patterns were carried out over a 2θ range of 3-50° using a D/max 2500/PC diffractometer with Cu K_α radiation (λ=1.5406 Å). High resolution transmission electron microscope (HRTEM) images were taken on JEM-2100F. Scanning electron microscope (SEM) images were taken on JSM-7600F (Japan). Fourier transform infrared (FT-IR) spectra were recorded in the 400~4000 cm^{-1} range on a German Bruke Tensor 27 Fourier transform-infrared spectrophotometer, using KBr pellets. UV-visible spectra (UV-vis) were collected in the 200~800 nm range on UV1700PC (Shanghai). Elemental analysis (C, H and N) was performed on a Vario EL III analyzer (Germany). Thermogravimetric data (TG) were obtained in nitrogen at 10°C/min in the 25~800°C on Perkin Elmer Pyris 1 instrument (America). Energy dispersive X-ray spectroscopy (EDX) measurements were carried out on Thermo Noran System7.

Electrochemical measurements were performed on a CHI660E electrochemical workstation (Chenhua, Shanghai). A conventional three-electrode system was used, with a bare/modified GCE as working electrode, platinum electrode as counter electrode, and KCl-saturated calomel electrode (SCE) as reference electrode. Phosphate buffer solution (PBS, 0.1 M, pH 7.0) was used as electrolyte, and was purged of oxygen with high purity nitrogen for at least 20 min prior to any experiments. Cyclic voltammetry (CV) conditions: initial potential (*E*): -0.1 V; final *E*: 1.0 V; initial scan: negative; scan rate: 0.1 V/s.

2.3 Synthesis of $[Cu_2(CoTCPP)(H_2O)_2]\cdot 0.5DMF\cdot 5H_2O$ (Cu-CoTCPP)

CoTCPP (0.01 mmol) and $Cu(NO_3)_2\cdot 3H_2O$ (0.02 mmol) were dissolved in a mixture of DMF (5.0 mL) and nitric acid (1.0 M, 4 mL). The mixture was sealed in Teflon lined autoclave and heated at 65 ℃ for 7 days. After slow cooling down to room temperature, the product was centrifuged and washed with DMF, EtOH, and H_2O, respectively. After drying at room temperature, $[Cu_2(CoTCPP)(H_2O)_2]\cdot 0.5DMF\cdot 5H_2O$ (Cu-CoTCPP) was obtained as purple powder.

2.4 Electrode modification

5 mg of Cu-CoTCPP was ultrasonically dispersed in 400 μL deionized water. 6 μL of this Cu-CoTCPP suspension was cast onto the surface of a pre-polished glassy carbon electrode (GCE, ∅ 3 mm) and dried in the air. Then 2 μL of 1% nafion solution was dropped to cover the electrode surface. After drying in the air, Cu-CoTCPP/GCE was obtained. In the case of Cu-CoTCPP/MWCNTs/GCE, similar

procedure was followed, except that 6 μL of suspension (5 mg/mL) of MWCNTs (length: >5 μm, diameter: 7~15 nm, purity: >97%, purchased from Shenzhen Nanotech Port Co., Ltd.) was cast onto the GCE surface and dried prior to the casting of Cu-CoTCPP.

3. Results and discussion

3.1 Characterization of Cu-CoTCPP

Figure 1 shows the schematic representation of Cu-CoTCPP and CoTCPP, which has been evidenced by the XRD result shown in Figure 2. The XRD result indicates that Cu-CoTCPP has a layered structure which is similar to CoTCPP-py-Cu (NAFS-1) [27] with the same plane structure but different interlayer spacing. The peaks in Fig. 2 marked with * at 7.5 (7.5), 19.5 (19.5), 21.4 (21.5), 23.2 (23.3), 30.5 (30.6), and 39.0 ° (39.0 °) for Cu-CoTCPP are consistent with those for NAFS-1 (shown in the following parentheses), which are respectively indexed as (110), (320), (400), (330), (440), and (550)/(710) on a metrically tetragonal unit cell with basal plane dimensions [27]. The layered structure model for NAFS-1 are composed of CoTCPP units linked by binuclear $Cu_2(COO)_4$ paddle-wheels [27]. The experimental XRD pattern of plane structure is in excellent agreement with the simulated powder XRD pattern of the plane structure model for NAFS-1 [27]. Therefore, it can be concluded that Cu-CoTCPP has a layered structure (Fig. 1A and B) similar to that of NAFS-1. The XRD pattern of NAFS-1 has three diffraction peaks at 9.3, 18.9, and 28.9 °, which can be indexed as (001), (002), and (003), suggesting that NAFS-1 has a layered structure and the interlayer spacing is 0.94 nm [27]. The peaks in Fig. 2 marked with ^ at 8.8 °, 17.8 °, and 36.5 ° are respectively indexed as (001), (002), and (004) for Cu-CoTCPP, indicating the layered structure with interlayer spacing of 1.0 nm, which is greater than the 0.94 nm for NAFS-1. The interdigitated layer stacking of NAFS-1 can be driven by attractive π-π interactions between adjacent Cu^{2+}-coordinated pyridine molecules that protrude from the 2D sheets [27], the absence of any coordinated pyridine molecules in Cu-CoTCPP led to the interdigitated layer stacking through van der Waals force, so the interlayer spacing is greater than the interlayer spacing of NAFS-1, meanwhile the absence of pyridine molecules led to the disappearance of peak at 11 ° (220) [27]. The absence of pyridine molecules in Cu-CoTCPP may be more suitable for biosensing. The enlarged interlayer space of this new bimetallic metalloporphyrinic framework allows the easy access of those analytes with dimeter small than 1 nm (for example, H_2O_2 or NO_2^-) to the catalytic active sites of Cu or Co ions. Overall, the XRD results show Cu-CoTCPP are composed of a similar 2D “checkerboard” motif of [5,10,15,20-(4-carboxyphenyl)porphyrin]Co(II) (CoTCPP) units linked by binuclear $Cu_2(COO)_4$ paddle-wheels and the interlayer spacing is 1.0 nm.

The IR spectra indicate that the CoTCPP struts are formed and suggest a bridging coordination mode of carboxyl group to copper. The IR spectra of CoTCPP and Cu-CoTCPP are shown in Fig. 3A. The absorption band at 1003 cm^{-1} for CoTCPP is assigned to the Co-N stretching vibration and the absorption bands at 825, 797, 766, and 716 cm^{-1} are assigned to the stretching vibration of porphyrin framework, which indicates the formation of the CoTCPP [28]. The absorptions at 1726 cm^{-1} are clearly due to the stretching vibration of the C=O of carboxylic acids and the absorptions at 1435 cm^{-1} due to the vibration of the O-H of carboxylic acids. Those peaks disappears in the IR spectrum of the Cu-CoTCPP, indicating that the four –COOH groups of CoTCPP ligand are all coordinated with Cu [9]. The peaks at 1604 and 1404 cm^{-1} are assigned to the symmetric (v^{s}_{coo-}) and antisymmetric (v^{as}_{coo-}) stretching vibration of the –COO^{-} groups. The Δν (v^{as}_{coo-} - v^{s}_{coo-}) is 200 cm^{-1}, indicating the high symmetry of the carboxyl group and suggesting a bridging coordination mode of carboxyl group to copper [23]. Summarily, four N from porphyrin ring of H_2TCPP coordinated with cobalt to form CoTCPP struts, and carboxyl groups from CoTCPP coordinated with copper to form a bridging coordination mode. Those results coincide with the structure of Cu-CoTCPP, which consists of CoTCPP units linked by binuclear $Cu_2(COO)_4$ paddle-wheels.

The Ultraviolet-visible (UV) absorption spectra confirm that the Co-N coordination bond and the Cu-carboxylate clusters exist in the Cu-CoTCPP. The UV absorption spectra of H_2TCPP, CoTCPP and Cu-CoTCPP in DMF are shown in Fig. 3B. The absorption spectrum of H_2TCPP (line a in Fig. 3B) is characteristic of free base porphyrins of D_{2h} symmetry in solution, displaying an intense Soret band in the near UV region which is centered at 419 nm and four low energy Q bands in the visible region occurring at 515, 549, 590, and 646 nm [28]. The absorption spectrum of CoTCPP is shown by line b in Fig. 3B. Upon chelation with a metal cobalt ion, the symmetry increases to D_{4h} and is accompanied by a red shift of the Soret band to 433 nm and collapse of the four Q-bands into two bands at 548 and 595 nm [29]. In comparison with the spectrum of CoTCPP in DMF solution, the Soret band of Cu-CoTCPP (line c in Fig. 3B) blue-shifts to 419 nm, while the two Q-bands convert into one band at 548, due to the formation of the Cu–O coordination bond between the copper ion and the oxygen atom from the carboxyl group of the corresponding porphyrin molecules [30]. The results prove that Co has been coordinated successfully with H_2TCPP and Cu has been coordinated successfully with carboxylic acids of CoTCPP molecules to form Cu-CoTCPP.

According to the results of TG and the elemental analysis, we conclude the formula of Cu-CoTCPP is $[Cu_2(Co\text{-}TCPP)(H_2O)_2]0.5DMF5H_2O$. The thermal property of Cu-CoTCPP was studied in the range of 22~800°C (Fig. S1). The thermogravimetric analysis indicated a weight loss of 7.5% over the temperature range 22~66°C, which can be attributed to the loss of 5 mol H_2O (the calculated result according to the formula $[Cu_2(CoTCPP)(H_2O)_2]0.5DMF5H_2O$ (calcd.) is 7.9%), 0.5 mol DMF was lost in the range of 66~114°C with weight loss of about 3.2% (calcd. 3.3%), the coordinated 2 mol H_2O were lost in the range of 114~278°C with a further weight loss of about 3.2% (calcd. 3.2%). Therefore, we conclude the formula is $[Cu_2(Co\text{-}TCPP)(H_2O)_2]0.5DMF5H_2O$. The elemental analysis was used to investigate the composition of the prepared products. The result showed that Cu-CoTCPP contained (wt%): C 52.85, N 5.26, H 3.68. And the calculated result according to the formula $[Cu_2(Co\text{-}TCPP)(H_2O)_2]0.5DMF5H_2O$ is C 52.46, N 5.56, H 3.69. The expermental data are in agreement with the theoretical values. The consistency between them suggests that the formula $[Cu_2(Co\text{-}TCPP)(H_2O)_2]\cdot 0.5DMF\cdot 5H_2O$ is resonable. In addition, the proportion of Cu and Co in Cu-CoTCPP is confirmed by the EDX as 2:1.

Electron microscope images (Fig. 4) show that particles are composed of stacked sheets. HRTEM image (Fig. 4A) of Cu-CoTCPP indicates that the obtained products are irregular particles, which are formed by stacking of a large number of sheets layer by layer. SEM images of Cu-CoTCPP in Fig. 4B and C further illustrate its morphology. Fig. 4B and C shows the SEM images of Cu-CoTCPP at different magnifications, which evidences again that the prepared Cu-CoTCPP is formed by stacking flakes. The size of flakes is around 200~300 nm.

3.2 Electrochemistry of Cu-CoTCPP

CV was used to investigate the electrochemistry property of Cu-CoTCPP. As shown in Fig. 5, there is only a smooth background curve for bare GCE (curve a, red solid line). For Cu-CoTCPP/GCE (curve b, blue solid line), there is a couple of redox peaks 1/1' which can be assigned to Cu^{II}/Cu^{I} [31, 32]. However, the reduction peak is larger than the oxidation peak. This is most possibly due to the instability of the reduced form of complex which may undergo a fast chemical oxidation [33]. Meanwhile, there is an irreversible oxidation peak 2 in the CV of Cu-CoTCPP/GCE, which can be assigned to the oxidation process of Co^{II}/Co^{III} [34].

The electrocatalysis of the Cu-CoTCPP/GCE towards H_2O_2 and NO_2^- was also investigated by CV. As shown in Fig. 6A, the oxidation current of bare GCE does not change when H_2O_2 was added: curve b (with H_2O_2) completely overlaps curve a (without H_2O_2). As for the modified electrode Cu-CoTCPP/GCE (curve c, without H_2O_2), both 1’ and 2 peaks increased significantly with the addition of H_2O_2 (curve d, with H_2O_2). This result shows that the active site of copper has electrocatalytic ability toward the reduction of H_2O_2. And the active site of cobalt has electrocatalytic ability toward the oxidation of H_2O_2. This result suggests that Cu-CoTCPP has bi-directional electrocatalytic ability toward both the reduction and oxidation of H_2O_2.

As shown in Fig. 6B, the current on bare GCE increases only very slightly at the potential of near 1.0 V when $NaNO_2$ was added (curve a and b). As for the modified electrode, Cu-CoTCPP/GCE, oxidation peak of Co^{II}/Co^{III} (curve c, without $NaNO_2$) increases significantly with the addition of $NaNO_2$ (curve d, with $NaNO_2$). This result suggests that the site of cobalt has electrocatalytic activity toward the oxidation of $NaNO_2$. However, the redox peaks of Cu^{II}/Cu^{I} are essentially unchanged, which shows the active site of copper has no obvious electrocatalytic ability toward $NaNO_2$.

These results suggest that both Cu and Co centers in Cu-CoTCPP/GCE have electrocatalytic activity. The copper center has electrocatalytic ability toward the reduction of H_2O_2 while the cobalt center has electrocatalytic ability toward the oxidation of H_2O_2 or $NaNO_2$. Therefore this sensor can be used to detect hydrogen peroxide or nitrite, respectively.

According to the CV results, -0.25 and 0.85 V were respectively chosen as constant reduction and oxidation potentials in chronoamperometry (Fig. S2) to investigate the performance of the modified electrode as a sensor towards H_2O_2. The better performance was obtained at the potential of -0.25 V, where the detection limit is 1.4×10^{-6} M and the linear range is 7.0×10^{-5} ~ 4.71×10^{-3} M (*R*=0.996), with a sensitivity of 28.5 mA mol^{-1} L cm^{-2}. At potential of 0.85 V, the corresponding data are 9.9×10^{-6} M, 5.8×10^{-5} ~ 1.56×10^{-2} M (*R*=0.997), and 4.23 mA mol^{-1} L cm^{-2}. The electrocatalytic activity of Cu-CoTCPP toward the reduction of H_2O_2 is higher than that toward the oxidation of it.

Fig. S3 shows the amperometric responses of the Cu-CoTCPP/GCE to successive addition of $NaNO_2$ at the potential of 0.85 V. The detection limit is 8.0×10^{-6} M and the linear range is 3.5×10^{-5} ~ 5.5×10^{-3}M (*R*=0.997), with a sensitivity of 15.32 mA mol^{-1} L cm^{-2}.

3.3 Electrochemistry of Cu-CoTCPP/MWCNTs

To improve the performance of the sensors, MWCNTs were added onto the GCE surface prior to the casting of Cu-CoTCPP, which may reduce the charge transfer resistance at the electrode surface and therefore increase the sensitivity of the modified electrodes, as is often done [23]. Fig. 7A compares CVs of bare GC electrode (a, red solid curve), Cu-CoTCPP/GCE, (b, blue dash curve), MWCNTs/GCE (c, black solid curve), and Cu-CoTCPP/MWCNTs/GCE (d, black dash curve). The background charge-discharge current on MWCNTs/GCE is increased greatly, which is due to the modification of MWCNTs and the resulted increased electrode area. More importantly, in Fig. 7A, the redox peak current of 1/1' on Cu-CoTCPP/MWCNTs/GCE (curve d) is much larger than that on

Cu-CoTCPP/GCE (curve b), which should be due to the reduce of the charge transfer resistance at the electrode surface. In order to evidence this point electrochemical impedance spectroscopy (EIS) of three kinds of electrodes (GC electrode, MWCNTs/GCE, and Cu-CoTCPP/MWCNTs/GCE) in 0.1 M KCl containing 5 mM $[Fe(CN)_6]^{4-/3-}$ was carried out and the results are shown in Fig. 7B. The diameter of semicircle at the high frequency is commonly used to evaluate the electron transfer resistance at the electrode surface, i.e., R_{ct} [36]. The larger diameter of the semicircle for GC electrode indicates a relative difficult interfacial electron transfer, or a larger R_{ct} of GC electrode. In comparison, there is almost no charge transfer resistance on MWCNTs/GCE or Cu-CoTCPP/MWCNTs/GCE, suggesting a fast electron transfer on the modified electrode surface.

Different from the CVs of Cu-CoTCPP/GCE in Fig. 6, a new pair of redox peaks 3/3’ at around 0.2 V appears in the CV of Cu-CoTCPP/MWCNTs/GCE (curve d in Fig. 7). It is also observed in the CV of MWCNTs/GCE (curve c) and assigned to the redox processes of the carboxyl group on MWCNTs [35]. Peaks 1/1’ and 2 were assigned to Cu^{II}/Cu^{I} and Co^{II}/Co^{III}, respectively, similar to those in the CVs of Cu-CoTCPP/GCE in Fig. 6. MWCNTs have stronger influence on the redox peaks of copper than on the oxidation peak of cobalt.

CVs of Cu-CoTCPP/MWCNTs/GCE (Fig. S4) indicate that the reduction current of Cu^{II} to Cu^{I} responding to H_2O_2 addition increases after MWCNTs were added, The reduction peak 1’ of curve c in Fig. S4 (without H_2O_2) increases obviously after H_2O_2 was added (curve d). However, both reduction and oxidation currents for

MWCNTs/GCE do not change when H_2O_2 was added (curve a and b). The result shows that MWCNTs has no obvious electrocatalytic ability toward H_2O_2. MWCNTs only improve the charge transport property of electrodes and make them more sensitive. The electrocatalytic active site for detection of H_2O_2 is still copper in Cu-CoTCPP. Addition of $NaNO_2$ has the similar influences on the oxidation peak of Co^{II}/Co^{III} on Cu-CoTCPP/MWCNTs/GCE and MWCNTs/GCE electrodes, suggesting that the cobalt center in Cu-CoTCPP is still active site for the detection of $NaNO_2$.

Due to its superior electrocatalytic activity discussed above, Cu-CoTCPP/MWCNTs/GCE was used for amperometric study. Fig. 8A shows the typical amperometric responses of the Cu-CoTCPP/MWCNTs/GCE to the successive addition of H_2O_2 at an applied potential of -0.25 V in 0.1 M PBS (pH 7.0). As can be seen from Fig. 8A, a good linear relationship was obtained between the reduction current (I_c) and concentration of H_2O_2 (C_H) from 5.0×10^{-7} to 6.2×10^{-3} M (I_c (μA) = (-11.86815 ± 0.10708) C_H (mM) + (-0.56706 ± 0.06929), R=0.999), the detection limit of 2.4×10^{-7} M was estimated at a signal-to-noise ratio of three, the detection sensitivity was 168 mA mol^{-1} L cm^{-2}.

The detection performance of Cu-CoTCPP/MWCNTs/GCE towards H_2O_2 was much better than those of Cu-CoTCPP/GCE (7.0×10^{-5} ~ 4.71×10^{-3} M (R=0.996), 1.4×10^{-6} M, 28.5 mA mol^{-1} L cm^{-2}, correspondingly). Obviously, MWCNTs had greatly improved the performance of the sensor. This sensor is also good in comparison with many other H_2O_2 sensors based on nanoscale noble metals and oxides. Not only its linear detection range extended to much lower concentration, but also its detection limit was lower than Ag/nichrome (5.8×10^{-7} M) [37], AgNPs-NFs(POPD)/GCE (6.2×10^{-5} M) [38] and $H_2TCPP-Fe_3O_4$ (1.07×10^{-6} M) [39]. Meanwhile, its sensitivity was higher than β-MnO_2 nanorods/GCE (21.74 mA mol^{-1} L cm^{-2}) [40]. The performance of Cu-CoTCPP/MWCNTs/GCE was somewhat similar to some sensors based on polymers containing Cu, such as $[Cu(tyr)_2]_n$/GCE [32] and GC/PVI/[Cu(2pymehist)Cl](ClO_4) [41]. Its detection limit was lower than those sensors based on CNTs, such as Hb-SWCNTs-CTAB (7.87×10^{-6} M) [42] and Mb-SWCNTs-CTAB (8.07×10^{-6} M) [42]. Its detection limit was also lower and the linear detection range extended to much lower concentration than HRP/PAn/MWCNTCOOH/Au (8.6×10^{-5} M, $8.6\times10^{-5}\sim1\times10^{-2}$ M) [20].

Fig. 8B shows the typical amperometric responses of the Cu-CoTCPP/MWCNTs/GCE to the successive addition of $NaNO_2$ at an applied potential of 0.85 V in 0.1M PBS (pH 7.0). A good linear relationship was obtained between the oxidation current (I_a) and different concentrations of $NaNO_2$ (C_N) from 2.5×10^{-6} to 1.1×10^{-3} M (I_a (μA) = (30.99495 ± 0.12659) C_N (mM) + (1.8654 ± 0.05469), R=0.9999), the detection limit of 1.7×10^{-7} M was estimated at a signal-to-noise ratio of three, the detection sensitivity was 439 mA mol^{-1} L cm^{-2}. The detection performance towards $NaNO_2$ was much better than those of Cu-CoTCPP/GCE ($3.5\times10^{-5}\sim5.5\times10^{-3}$ M (R=0.997), 8.0×10^{-6} M, 15.32 mA mol^{-1} L cm^{-2}, correspondingly). Compared with other electrochemical sensors to nitrite such as noble metals, nanotube composites and Co-containing compounds, its performance is improved. Its sensitivity is higher than Au-PEI/GO/GCE (411 mA mol^{-1} L cm^{-2})

[43]. Its linear detection range is extended to much lower concentration than PEDOT-AuNPs (3.0×10^{-6} ~ 3×10^{-3} M) [44] and RGO–MWCNTs/GCE (7.5×10^{-5} ~ -6.06×10^{-3} M) [21]. Its detection limit was also lower than RGO–MWCNTs/GCE (2.5×10^{-5} M) [21].

The selectivity, stability, and reproducibility of the sensor were also investigated. Although it is well known that some potentially coexisting compounds such as K^+, Cl^-, NO_3^-, Ac^-, Zn^{2+}, Mg^{2+}, UA (uric acid) and Glu (glucose) in the biological system will affect the sensor response [45], they do not significantly disturb the determination of H_2O_2 and NO_2^- as shown in Fig. S5 and 6. Citric acid and ascorbic acid (AA) do not disturb the determination of NO_2^-, but disturb the determination of H_2O_2 slightly as shown in Fig. S7 and 8. However, dopamine disturbs the determination of NO_2^- seriously.

The electrode still maintained 95.6% of its response after preserved under ambient condition for 36 days. The relative standard deviation (RSD) for 6 detection results from parallel electrodes was 6.9%.

To demonstrate the applicability of this sensor for the analysis of the sample, it was applied to determine H_2O_2 or NO_2^- in artificial samples. The recovery test was performed by standard-addition method. The results are summarized in Table 1 and Table 2.

In summary, this electrochemical sensor based on Cu-CoTCPP/MWCNTs/GCE can be used for the determination of hydrogen peroxide and nitrite without significant interference. Cu-CoTCPP/MWCNTs/GCE showed general superiorities over other reported sensors: such as fast response, high steadiness, and cheapness. Meanwhile, high sensitivity and selectivity were retained as well. The high sensitivity, stability, or reproducibility of this Cu-CoTCPP/MWCNTs/GCE sensor should be mainly related to the special structure of Cu-CoTCPP, which is composed of a 2D “checkerboard” motif of CoTCPP units linked by binuclear $Cu_2(COO)_4$ paddle-wheels with a interlayer spacing of 1.0 nm. This structure allows the convenient access of analytes to the catalytic centers and also avoid the leaching of catalytic ions or the agglomeration of catalytic centers.

4. Conclusions

In summary, we successfully synthesized a bimetallic metalloporphyrinic framework Cu-CoTCPP with interesting electrocatalytic property. It is constructed from CoTCPP units bridged by binuclear $Cu_2(COO)_4$ paddle-wheels. Based on an overall consideration of various characterizations, including XRD, TEM, SEM, IR, UV-vis, TG, and elemental analysis, it can be deduced that Cu-CoTCPP is a new coordination polymer with a formula of $[Cu_2(Co\text{-}TCPP)(H_2O)_2]\cdot 0.5DMF\cdot 5H_2O$. Very interestingly, Cu-CoTCPP/GCE showed electrocatalytic ability toward the reduction of H_2O_2 and oxidation of NO_2^-. Furthermore, the addition of MWCNTs improved the electrode’s sensitivity. -0.25 V was chosen to obtain good performance for reductive determination of H_2O_2 and 0.85 V was chosen to obtain good performance for oxidative determination of NO_2^-. Cu-CoTCPP /MWCNTs/GCE showed fast response to H_2O_2 and NO_2^- and had a quite low detection limit of 2.4×10^{-7} M, a wide linear range of $5.0\times10^{-7} \sim 6.2\times10^{-3}$ M and a high sensitivity of 168 mA mol^{-1} L cm^{-2} for H_2O_2, meanwhile it also had a lower detection limit of 1.7×10^{-7} M, a linear range of $2.5\times10^{-6} \sim 1.1\times10^{-3}$ M and a higher sensitivity of 439 mA mol^{-1} L cm^{-2} for NO_2^-. In addition, it also had good selectivity, high stability and reproducibility.

Acknowledgements

The authors thank National Natural Science Foundation of China (Grant No. 21175068 and 21335004) for the financial support. We also thank the Priority Academic Program Development of Jiangsu Higher Education Institutions.

References

[1] O.M. Yaghi, M. O'Keeffe, N.W. Ockwig, H.K. Chae, M. Eddaoudi, J. Kim, Reticular synthesis and the design of new materials, Nature 423 (2003) 705-714.

[2] G. Férey, Hybrid porous solids: past, present, future, Chemical Society Reviews 37 (2008) 191-214.

[3] S. Kitagawa, R. Kitaura, S. Noro, Functional porous coordination polymers, Angewandte Chemie-International Edition 43 (2004) 2334-2375.

[4] J.S. Seo, D. Whang, H. Lee, S.I. Jun, J. Oh, Y.J. Jeon, K. Kim, A homochiral metal-organic porous material for enantioselective separation and catalysis, Nature 404 (2000) 982-986.

[5] F. Raganati, V. Gargiulo, P. Ammendola, M. Alfe, R. Chirone, CO 2 capture performance of HKUST-1 in a sound assisted fluidized bed, Chemical Engineering Journal 239 (2014) 75-86.

[6] J. Peng, S. Xian, J. Xiao, Y. Huang, Q. Xia, H. Wang, Z. Li, A supported Cu (I)@ MIL-100 (Fe) adsorbent with high CO adsorption capacity and CO/N 2 selectivity,

Chemical Engineering Journal 270 (2015) 282-289.

[7] Q.W. Li, W.Y. Zhang, O.S. Miljanic, C.H. Sue, Y.L. Zhao, L.H. Liu, C.B. Knobler, J.F. Stoddart, O.M. Yaghi, Docking in Metal-Organic Frameworks, Science 325 (2009) 855-859.

[8] I. Goldberg, Crystal engineering of porphyrin framework solids, Chemical Communications (2005) 1243-1254.

[9] E.-Y. Choi, P.M. Barron, R.W. Novotny, H.-T. Son, C. Hu, W. Choe, Pillared Porphyrin Homologous Series: Intergrowth in Metal-Organic Frameworks, Inorg. Chem 48 (2009) 426-428.

[10] M.E. Kosal, J.-H. Chou, S.R. Wilson, K.S. Suslick, A functional zeolite analogue assembled from metalloporphyrins, Nat. Mater. 1 (2002) 118-121.

[11] A.M. Shultz, O.K. Farha, J.T. Hupp, S.T. Nguyen, A Catalytically Active, Permanently Microporous MOF with Metalloporphyrin Struts, Journal of the American Chemical Society 131 (2009) 4204-+.

[12] R.A. Sheldon, Metalloporphyrins in Catalytic Oxidations, Marcel Dekker (1994).

[13] J.Y. Liu, X.F. Li, Z.X. Guo, Y.Z. Li, A.J. Huang, W.B. Chang, Comparative study on heme-containing enzyme-like catalytic activities of water-soluble metalloporphyrins, Journal of Molecular Catalysis a-Chemical 179 (2002) 27-33.

[14] M. Vago, V. Campodall'Orto, I. Rezzano, E.S. Forzani, E.J. Calvo, Metalloporphyrin electropolymerization: electrochemical quartz crystal microgravimetric studies, Journal of Electroanalytical Chemistry 566 (2004) 177-185.

[15] R.F.P. Nogueira, M.C. Oliveira, W.C. Paterlini, Simple and fast spectrophotometric determination of H2O2 in photo-Fenton reactions using metavanadate, Talanta 66 (2005) 86-91.

[16] T.A. Doane, W.R. Horwath, Spectrophotometric determination of nitrate with a single reagent, Analytical Letters 36 (2003) 2713-2722.

[17] R.T. Masserini, K.A. Fanning, A sensor package for the simultaneous determination of nanomolar concentrations of nitrite, nitrate, and ammonia in seawater by fluorescence detection, Marine Chemistry 68 (2000) 323-333.

[18] S. Hanaoka, J.M. Lin, M. Yamada, Chemiluminescent flow sensor for H2O2

based on the decomposition of H2O2 catalyzed by cobalt(II)-ethanolamine complex immobilized on resin, Analytica Chimica Acta 426 (2001) 57-64.

[19] M.K. Amini, M. Pourhossein, M. Talebi, A chemiluminescence flow injection system for nitrite ion determination, Journal of the Iranian Chemical Society 2 (2005) 305-314.

[20] M.Y. Hua, Y.C. Lin, R.Y. Tsai, H.C. Chen, Y.C. Liu, A hydrogen peroxide sensor based on a horseradish peroxidase/polyaniline/carboxy-functionalized multiwalled carbon nanotube modified gold electrode, Electrochimica Acta 56 (2011) 9488-9495.

[21] F. Hu, S. Chen, C. Wang, R. Yuan, D. Yuan, C. Wang, Study on the application of reduced graphene oxide and multiwall carbon nanotubes hybrid materials for simultaneous determination of catechol, hydroquinone, p-cresol and nitrite, Analytica Chimica Acta 724 (2012) 40-46.

[22] B. Zhou, L.M. Liang, J. Yao, Effects of isomorphous substitution of a coordination polymer on the properties and its application in electrochemical sensing, Journal of Solid State Chemistry 215 (2014) 109-113.

[23] J. Yang, B. Zhou, J. Yao, X.-Q. Jiang, Nanorods of A New Metal-Biomolecule Coordination Polymer Showing Novel Bidirectional Electrocatalytic Activity and Perfect Performance in Electrochemical Sensing, Biosensors and Bioelectronics 67 (2015) 66-72.

[24] E.C. Zhou, Y.W. Zhang, Y.J. Li, X.W. He, Cu(II)-Based MOF Immobilized on Multiwalled Carbon Nanotubes: Synthesis and Application for Nonenzymatic Detection of Hydrogen Peroxide with High Sensitivity, Electroanalysis 26 (2014) 2526-2533.

[25] J.S. Lindsey, H.C. Hsu, I.C. Schreiman, SYNTHESIS OF TETRAPHENYLPORPHYRINS UNDER VERY MILD CONDITIONS, Tetrahedron Letters 27 (1986) 4969-4970.

[26] A. Kumar, S. Maji, P. Dubey, G.J. Abhilash, S. Pandey, S. Sarkar, One-pot general synthesis of metalloporphyrins, Tetrahedron Letters 48 (2007) 7287-7290.

[27] R. Makiura, S. Motoyama, Y. Umemura, H. Yamanaka, O. Sakata, H. Kitagawa, Surface nano-architecture of a metal–organic framework, Nat. Mater. 9 (2010)

565-571.

[28] M. Gouterman, Spectra of porphyrins, Journal of Molecular Spectroscopy 6 (1961) 138-163.

[29] S.R. Ahrenholtz, C.C. Epley, A.J. Morris, Solvothermal Preparation of an Electrocatalytic Metalloporphyrin MOF Thin Film and its Redox Hopping Charge-Transfer Mechanism, Journal of the American Chemical Society 136 (2014) 2464-2472.

[30] S. Tanaka, M. Shirakawa, K. Kaneko, M. Takeuchi, S. Shinkai, Porphyrin-based organogels: Control of the aggregation mode by a pyridine-carboxylic acid interaction, Langmuir 21 (2005) 2163-2172.

[31] Y.-T. Li, W. Sun, Y.-J. Zheng, Z.-Y. Wu, C.-W. Yan, Synthesis, Structure and Cyclic Voltammetry Studies of a 2D Sheet-like μ3-Hydroxyl- and μ2-, μ4-Oxamidato-Bridged Copper(II) Complex, Journal of Inorganic and Organometallic Polymers and Materials 21 (2010) 182-188.

[32] B. Zhou, F.C. Xu, J. Yang, J. Yao, Y.H. Xiao, Ultrasound-assisted synthesis of nanoscale coordination polymers and their application as enzyme-free electrochemical biosensors for H2O2, Materials Letters 107 (2013) 206-209.

[33] X. Wang, H. Zhao, H. Lin, G. Liu, J. Fang, B. Chen, Renewable New Copper Complex Bulk-Modified Carbon Paste Electrode: Preparation, Electrochemistry, and Electrocatalysis, Electroanalysis 20 (2008) 1055-1060.

[34] M.H. Habibi, E. Shojaee, Y. Yamane, T. Suzuki, Synthesis, Spectroscopic Studies, Crystal Structure and Electrochemical Properties of New Cobalt(III) Complex Derived from 2-Aminophenol and 4-(Dimethylamino)Cinnamaldehyde: Nano-Sized Complex Thin Film Formation via Surface Layer-by-Layer Chemical Deposition Method, Journal of Inorganic and Organometallic Polymers and Materials 22 (2011) 190-195.

[35] H. Lund, O. Hammerich, Organic electrochemistry, M. Dekker, New York, 2001.

[36] S. Qi, B. Zhao, H. Tang, X. Jiang, Determination of ascorbic acid, dopamine, and uric acid by a novel electrochemical sensor based on pristine graphene, Electrochimica Acta, 161 (2015) 395-402.

[37] W. Zhao, Z. Wang, Q. Li, Fabrication of a nichrome electrode coated with silver microcrystals, and its application to sensing hydrogen peroxide, Analytical Methods 4 (2012) 1105.

[38] J. Tian, S. Liu, X. Sun, Supramolecular Microfibrils ofo-Phenylenediamine Dimers: Oxidation-Induced Morphology Change and the Spontaneous Formation of Ag Nanoparticle Decorated Nanofibers, Langmuir 26 (2010) 15112-15116.

[39] Q. Liu, H. Li, Q. Zhao, R. Zhu, Y. Yang, Q. Jia, B. Bian, L. Zhuo, Glucose-sensitive colorimetric sensor based on peroxidase mimics activity of porphyrin-Fe3O4 nanocomposites, Materials Science and Engineering: C 41 (2014) 142-151.

[40] A.-J. Wang, P.-P. Zhang, Y.-F. Li, J.-J. Feng, W.-J. Dong, X.-Y. Liu, Hydrogen peroxide sensor based on glassy carbon electrode modified with β-manganese dioxide nanorods, Microchimica Acta 175 (2011) 31-37.

[41] W.A. Alves, I.O. Matos, P.M. Takahashi, E.L. Bastos, H. Martinho, J.G. Ferreira, C.C. Silva, R. Santos, A. Paduan, A.M.D. Ferreira, A Chloro-Bridged Linear Chain Imine-Copper(II) Complex and Its Application as an Enzyme-Free Amperometric Biosensor for Hydrogen Peroxide, European Journal of Inorganic Chemistry (2009) 2219-2228.

[42] S. Wang, F. Xie, G. Liu, Direct electrochemistry and electrocatalysis of heme proteins on SWCNTs-CTAB modified electrodes, Talanta 77 (2009) 1343-1350.

[43] B. Yuan, C. Xu, L. Liu, Y. Shi, S. Li, R. Zhang, D. Zhang, Polyethylenimine-bridged graphene oxide–gold film on glassy carbon electrode and its electrocatalytic activity toward nitrite and hydrogen peroxide, Sensors and Actuators B: Chemical 198 (2014) 55-61.

[44] O. Zhang, Y. Wen, J. Xu, L. Lu, X. Duan, H. Yu, One-step synthesis of poly(3,4-ethylenedioxythiophene)–Au composites and their application for the detection of nitrite, Synthetic Metals 164 (2013) 47-51.

[45] C. Wang, X.C. Zou, Q. Wang, K.Y. Shi, J. Tan, X. Zhao, Y.Q. Chai, R. Yuan, A nitrite and hydrogen peroxide sensor based on Hb adsorbed on Au nanorods and graphene oxide coated by polydopamine, Analytical Methods 6 (2014) 758-765.

Figure Captions

Fig. 1. Schematic representation of Cu-CoTCPP (A) in top view, (B) in side view, and (C) schematic representation of CoTCPP.

Fig. 2. The XRD diffraction pattern of Cu-CoTCPP.

Fig. 3. (A) FTIR spectra of CoTCPP (a) and Cu-CoTCPP (b). (B) UV-vis absorption spectra of H_2TCPP (a), CoTCPP (b), and Cu-CoTCPP (c) in DMF.

Fig. 4. (A) HRTEM image, (B, C) SEM images of the Cu-CoTCPP.

Fig. 5. CVs of bare GC electrode (a) and Cu-CoTCPP/GC electrode (b) in 4 mL N_2-saturated PBS (0.1 mol L^{-1}, pH 7.0). The scan rate: 100 mV s^{-1}.

Fig. 6. (A) CVs of bare GC (a, b) and Cu-CoTCPP/GC (c, d) electrode without H_2O_2 (a, c) and with 0.5 mmol L^{-1} H_2O_2 (b, d). (B) CVs of bare GC (a, b) and Cu-CoTCPP/GC (b, d) electrode without $NaNO_2$ (a, c) and with 0.25 mmol L^{-1} $NaNO_2$ (b, d). All CVs were carried out in 4 mL N_2-saturated PBS (0.1 mol L^{-1}, pH 7.0). The scan rate: 100 mV s^{-1}.

Fig. 7. (A) CVs of bare GC electrode (a, red solid curve), Cu-CoTCPP/GCE, (b, blue dash curve), MWCNTs/GCE (c, black solid curve), and Cu-CoTCPP/MWCNTs/GCE

(d, black dash curve) in N_2-saturated PBS (0.1 mol L^{-1}, pH 7.0). The scan rate: 100 mV s^{-1}. (B) EIS of GC electrode, MWCNTs/GCE, and Cu-CoTCPP/MWCNTs/GCE in 0.1 M KCl containing 5 mM $[Fe(CN)_6]^{4-/3-}$. The frequency range is from 0.01 Hz to 100 kHz.

Fig. 8. Amperometric responses of Cu-CoTCPP/MWCNTs/GCE to successive addition of H_2O_2 (A) at -0.25 V or $NaNO_2$ (B) at 0.85 V in 4 mL N_2-saturated PBS (0.1 M, pH 7.0). Inset: the corresponding linear curves of currents versus the concentration of H_2O_2 and $NaNO_2$.

Table Captions

Table 1. Determination of H_2O_2 in the artificial samples and the recovery.

Table 2. Determination of $NaNO_2$ in the artificial samples and the recovery

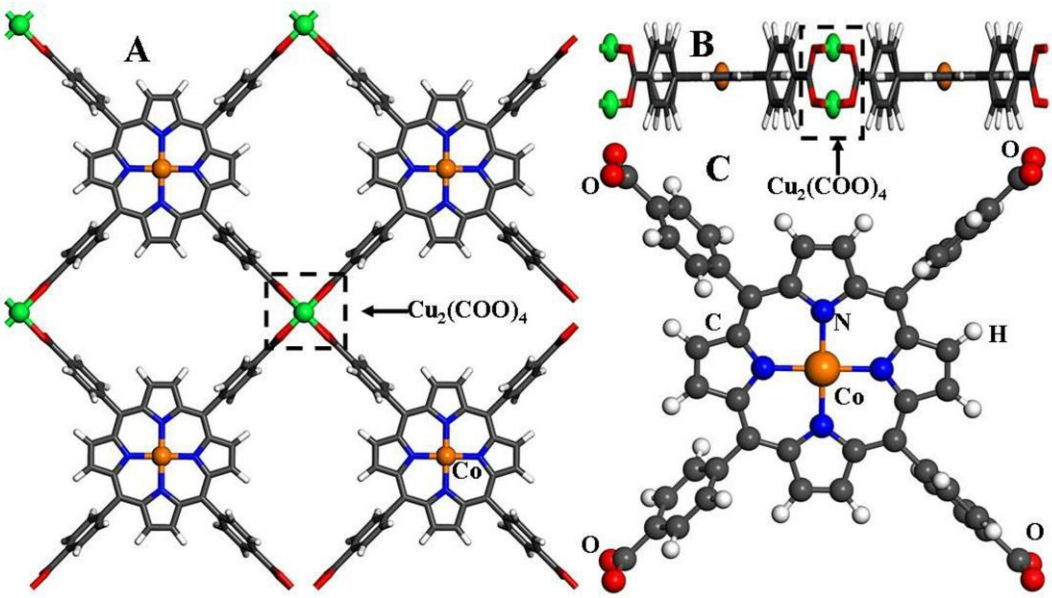

Fig. 1. Schematic representation of Cu-CoTCPP (A) in top view, (B) in side view, and (C) schematic representation of CoTCPP.

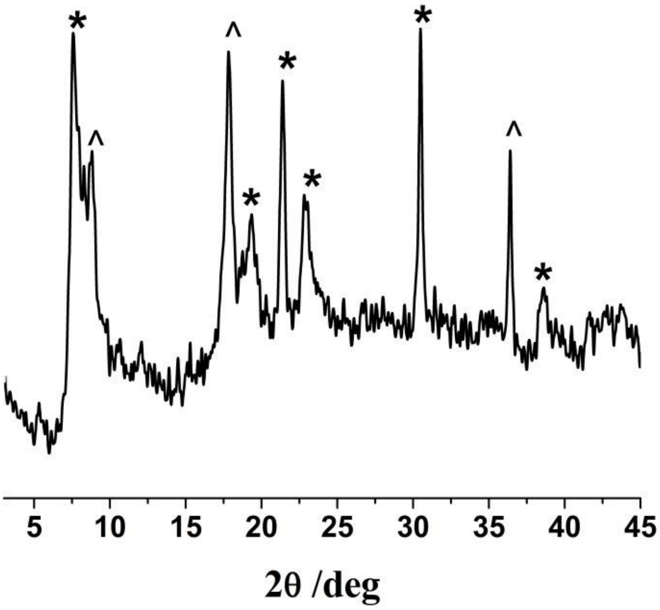

Fig. 2. The XRD diffraction pattern of Cu-CoTCPP.

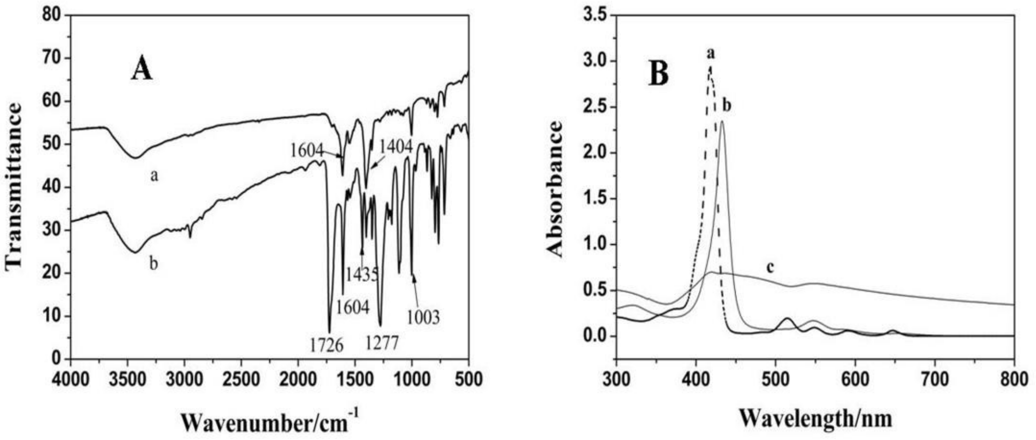

Fig. 3. (A) FTIR spectra of CoTCPP (a) and Cu-CoTCPP (b). (B) UV-vis absorption spectra of H_2TCPP (a), CoTCPP (b), and Cu-CoTCPP (c) in DMF.

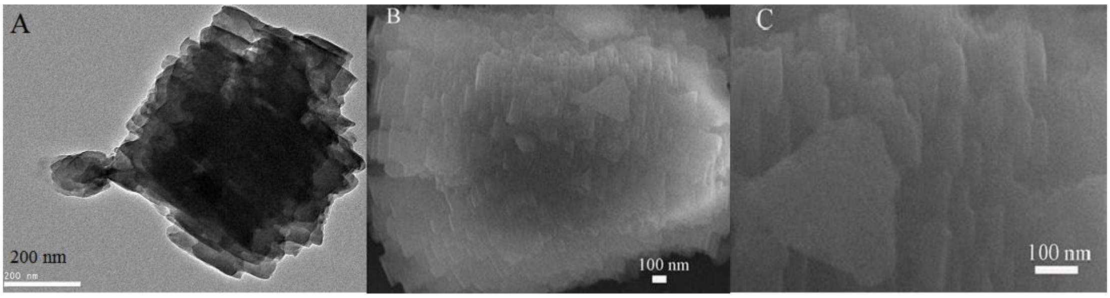

Fig. 4. (A) HRTEM image, (B, C) SEM images of the Cu-CoTCPP.

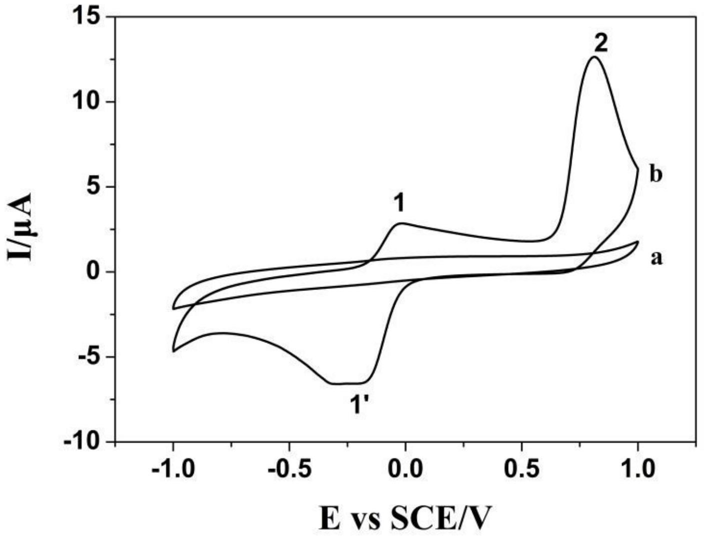

Fig. 5. CVs of bare GC electrode (a) and Cu-CoTCPP/GC electrode (b) in 4 mL N_2-saturated PBS (0.1 mol L^{-1}, pH 7.0). The scan rate: 100 mV s^{-1}.

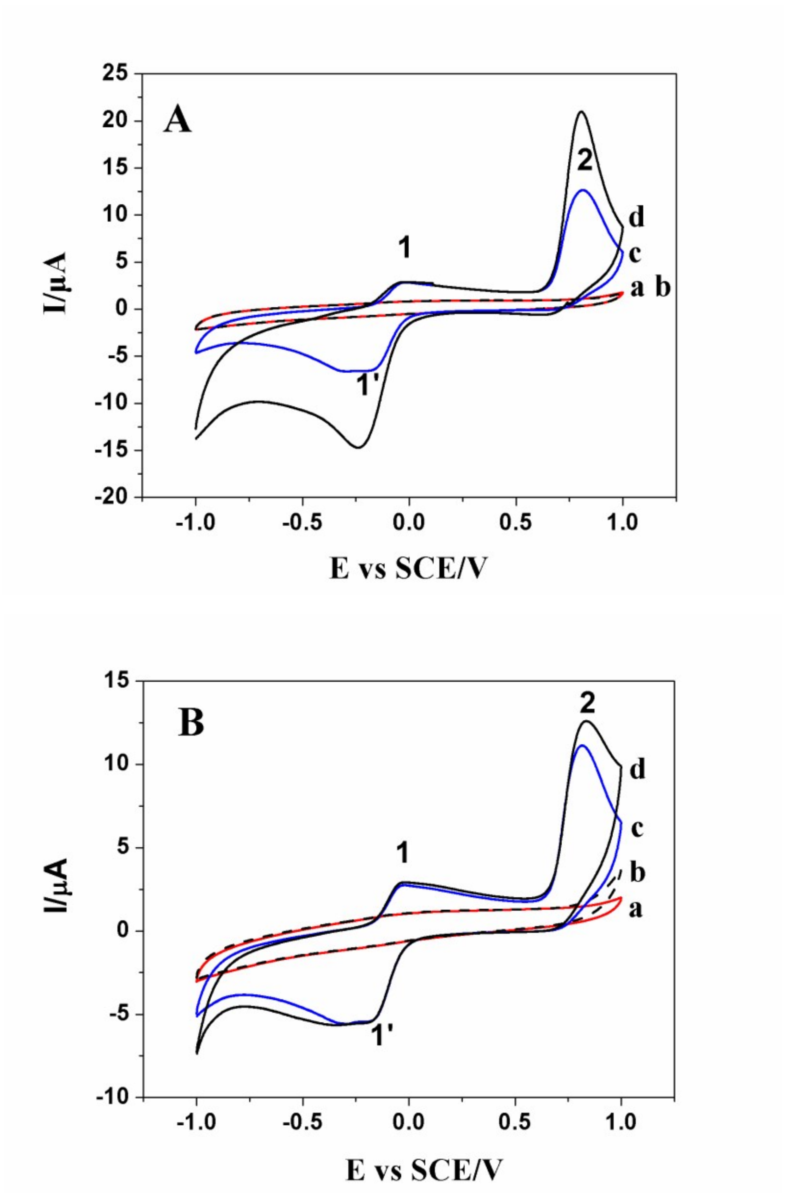

Fig. 6. (A) CVs of bare GC (a, b) and Cu-CoTCPP/GC (c, d) electrode without H_2O_2 (a, c) and with 0.5 mmol L^{-1} H_2O_2 (b, d). (B) CVs of bare GC (a, b) and Cu-CoTCPP/GC (b, d) electrode without $NaNO_2$ (a, c) and with 0.25 mmol L^{-1} $NaNO_2$ (b, d). All CVs were carried out in 4 mL N_2-saturated PBS (0.1 mol L^{-1}, pH 7.0). The scan rate: 100 mV s^{-1}.

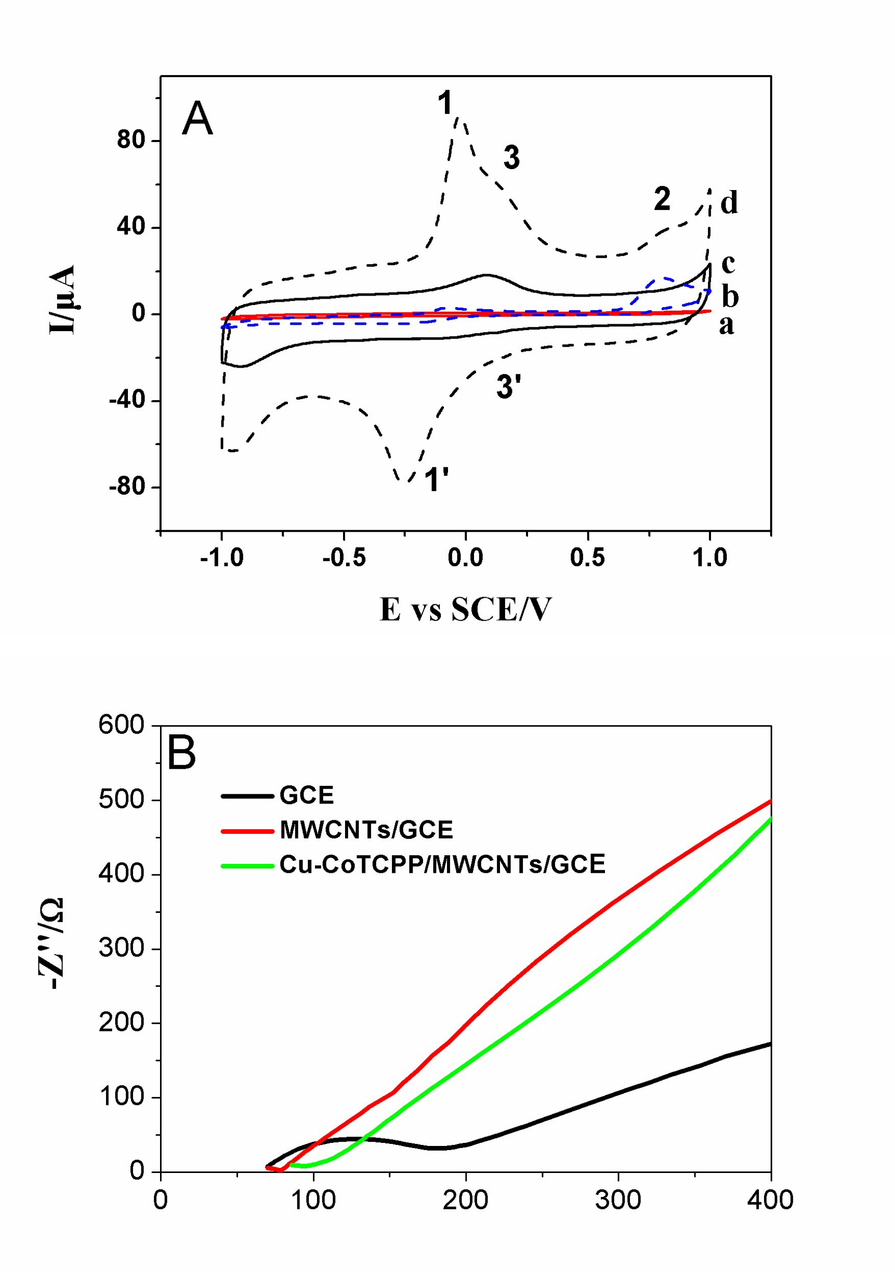

Fig. 7. (A) CVs of bare GC electrode (a, red solid curve), Cu-CoTCPP/GCE, (b, blue dash curve), MWCNTs/GCE (c, black solid curve), and Cu-CoTCPP/MWCNTs/GCE (d, black dash curve) in N_2-saturated PBS (0.1 mol L^{-1}, pH 7.0). The scan rate: 100 mV s^{-1}. (B) EIS of GC electrode, MWCNTs/GCE, and Cu-CoTCPP/MWCNTs/GCE in 0.1 M KCl containing 5 mM $[Fe(CN)_6]^{4-/3-}$. The frequency range is from 0.01 Hz to 100 kHz.

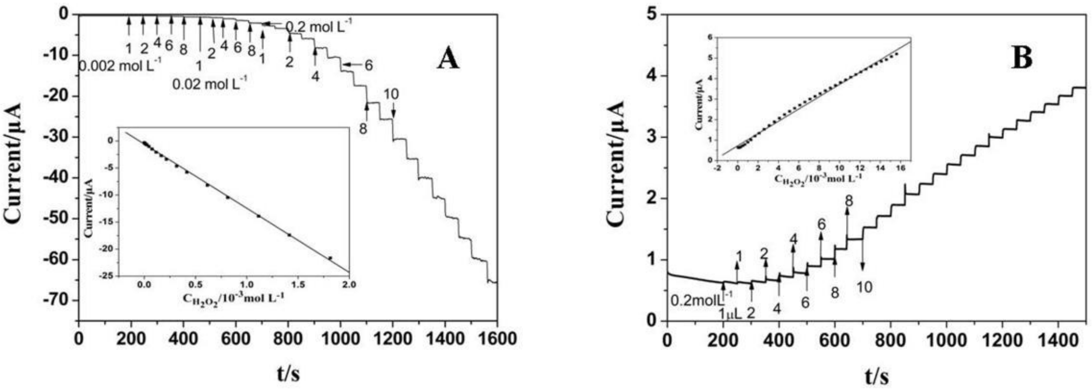

Fig. 8. Amperometric responses of Cu-CoTCPP/MWCNTs/GCE to successive addition of H_2O_2 (A) at -0.25 V or $NaNO_2$ (B) at 0.85 V in 4 mL N_2-saturated PBS (0.1 M, pH 7.0). Inset: the corresponding linear curves of currents versus the concentration of H_2O_2 and $NaNO_2$.

Table 1. Determination of H_2O_2 in the artificial samples and the recovery

Sample	Sample Concen./mM	Added/mM	Found/mM	Recovery(%)	RSD (%)
1	0.25	0.25	0.22	88	20.2
	0.25	0.50	0.61	122	19.1
2	0.50	0.50	0.47	94	14.8
	0.50	1.00	1.00	100	12.4

Table 2. Determination of $NaNO_2$ in the artificial samples and the recovery

Sample	Sample Concen./mM	Added/mM	Found/mM	Recovery(%)	RSD (%)
1	0.25	0.25	0.19	76	6.3
	0.25	0.50	0.53	106	2.5
2	0.50	0.50	0.55	110	4.9
	0.50	1.00	1.13	113	10.5

A table of contents entry:

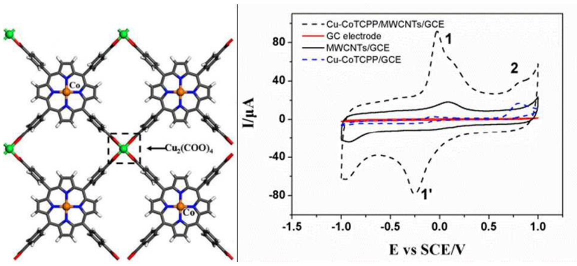

Bimetallic electrocatalytic ability of a new metallic porphyrin, Cu-CoTCPP, toward redox of H_2O_2 and oxidation of $NaNO_2$.